ENVIRONMENTAL RESEARCH
LETTERS

LETTER • OPEN ACCESS

Rapid restratification of the ocean surface boundary layer during the suppressed phase of the MJO in austral spring

To cite this article: Je-Yuan Hsu *et al* 2022 *Environ. Res. Lett.* **17** 024031

IOP Publishing Environ. Res. Lett. 17 (2022) 024031 https://doi.org/10.1088/1748-9326/ac4f11

ENVIRONMENTAL RESEARCH
LETTERS

OPEN ACCESS

RECEIVED
14 September 2021

REVISED
19 January 2022

ACCEPTED FOR PUBLICATION
26 January 2022

PUBLISHED
11 February 2022

LETTER

Rapid restratification of the ocean surface boundary layer during the suppressed phase of the MJO in austral spring

Je-Yuan Hsu[1,*], **Ming Feng**[2,3] **and Susan Wijffels**[4]

[1] Institute of Oceanography, National Taiwan University, Taipei, Taiwan
[2] CSIRO Oceans and Atmosphere, Perth, Australia
[3] Centre for Southern Hemisphere Oceans Research (CSHOR), Hobart, Australia
[4] Woods Hole Oceanographic Institution, Woods Hole, United States of America
[*] Author to whom any correspondence should be addressed.

E-mail: jyahsu@ntu.edu.tw

Keywords: importance of upper ocean stratified layers in air-sea interaction, 3D restratification processes near the sea surface, strong diurnal variations of SST, MJO-ocean interaction during the suppressed phase of MJOs, rapid restratification of the ocean surface boundary layer

Supplementary material for this article is available online

Abstract

Rapid restratification of the ocean surface boundary layer in the Indonesian-Australian Basin was captured in austral spring 2018, under the conditions of low wind speed and clear sky during the suppressed phase of Madden–Julian Oscillations (MJOs). Despite sunny days, strong diurnal variations of sea surface temperature (SST) were not observed until the wind speed became extremely low, because the decreasing wind speed modulated the latent heat flux. Combined with the horizontal advection of ocean current, the reduced upward heat loss inhibited the nighttime convective mixing and facilitated the restratification of the subsurface ocean layers. The surface mixed layer was thus shoaled up to 40 m in two days. The restratified upper ocean then sustained high SSTs by trapping heat near the sea surface until the onset of the MJO convection. This restratification process might be initialized under the atmospheric downwelling conditions during the suppressed phase of MJOs. The resulted high SSTs may affect the development and trajectories of MJOs, by enhancing air-sea heat and moisture fluxes as the winds pick up. Simulating this detailed interaction between the near-surface ocean and atmospheric features of MJOs remains a challenge, but with sufficient vertical resolution and realistic initial conditions, several features of the observations can be well captured.

1. Introduction

Madden–Julian Oscillations (MJOs; Shinoda and Hendon 1998, Zhang 2005, Moum *et al* 2014, Seo *et al* 2014) are intraseasonal-varying weather systems that can significantly affect the onset and timing of monsoon precipitation around the Maritime Continent. Under the influences of atmospheric general circulation associated with the suppressed phase of MJOs, the tropical warm pools frequently feature low wind speed and clear sky conditions, favorable for the occurrence of strong diurnal variations of sea surface temperature (SST. Sutherland *et al* 2016, Moulin *et al* 2018, Thompson *et al* 2019, Hughes *et al* 2020). Several model studies have demonstrated that significant SST warming can enhance air-sea heat and moisture fluxes, and thereby the development and propagation of MJOs (Bernie *et al* 2008, DeMott *et al* 2015, Ruppert and Johnson 2015). Note that fine-scale turbulence driven by nighttime convection and vertical shear of horizontal current can cool SST by entraining cold water from the stratified subsurface layers to the sea surface. Exploring the complicated interaction between the upper ocean stratified layers and atmospheric features of MJOs can benefit the forecast of intraseasonal weather systems.

Brainerd and Gregg (1995) define a 'surface mixed layer' (ML), spanning from the sea surface to the top of the seasonal thermocline, as a layer recently well-mixed by turbulence. However, fluxes on different

timescales can affect the density stratification in the ML, resulting in a more complex picture. During the daytime, the absorption of penetrative solar radiation can form a diurnal warm layer that sits over a diurnal thermocline near the sea surface (Kudryavtsev and Soloviev 1990). A residual layer (RL) which spans from the bottom of the diurnal thermocline to the top of the seasonal thermocline, can be restratified by the downward heat fluxes (including the penetrative solar flux), lateral advection, and turbulent mixing (Brainerd and Gregg 1993, Kunze *et al* 2021). Nighttime convective mixing typically destratifies all these layers at the end of a diurnal cycle. On timescales longer than diurnal variations, lateral advection driven by the frontogenesis of submesoscale fronts or wind may restratify the ocean surface boundary layer (Johnson *et al* 2016, 2020). The sharp horizontal buoyancy gradient at the fronts provides the available potential energy for inducing the submesoscale eddy instability (Boccaletti *et al* 2007, Fox-Kemper *et al* 2008). Hence, the restratification of ML may involve complicated processes.

Many previous studies have discussed the restratification of the ocean surface boundary layer around springtime (e.g. Mahadevan *et al* 2010, 2012, Johnson *et al* 2016). In winter, strong wind and radiative cooling destratifies the seasonal thermocline and deepens the ML. From winter to summer, the increasing insolation will enhance the upper ocean heat content. The heat captured in the diurnal warm layer will be redistributed through the deeper ML by nighttime convective mixing. It can gradually increase the daily-mean SST and the stratification across the base of the diurnal warm layer. The increased density stratification in the upper ocean will trap more heat in a shallower ML by inhibiting turbulent mixing (Sui *et al* 1997). MJOs propagating along the equator after October in boreal autumn-winter (Moum *et al* 2014) will experience the seasonal transition of the Southern Hemisphere ocean. Because the shoaling of ML can affect the daily-mean SST (Bernie *et al* 2005), it is important to explore the interaction between the MJOs and the restratification of the ocean surface boundary layer around tropical warm pools.

This study documents observations of SST warming of >1 °C in two days during the suppressed phase of one MJO event (Feng *et al* 2020), which is more rapid compared to the previous observations for MJOs (e.g. <1 °C in ten days in Moum *et al* 2014). The thickness of ML changes up to 40 m, more significantly than that during the seasonal transition from spring to summer (e.g. ∼20 m in ten days in Large *et al* 1994). The high SSTs (>27.5 °C), sustained by the rapid restratification of the ocean surface boundary layer, can enhance the heat and moisture fluxes to the atmosphere. In the following, our observations will be described in section 2. The evolution of stratified layers in the upper ocean is presented in section 3. Section 4 describes numerical model simulations of the upper ocean response to prescribed atmospheric forcing, which are then used to explore the dynamics behind the rapid restratification of the ocean surface boundary layer.

2. Observations in the field experiment

In November 2018, a collaborative field campaign between Centre for Southern Hemisphere Oceans Research (CSHOR) and China's First Institution of Oceanography was conducted to explore the air-sea interaction in the Indonesian-Australian Basin (Feng *et al* 2020). A shelf version of the Bailong buoy system (supporting information A available online at stacks.iop.org/ERL/17/024031/mmedia) was deployed off the northwest coast of Australia, along with six rapid profiling ALAMO floats from MRV Systems and two Teledyne Web EM-APEX floats. The ALAMO floats measured the seawater temperature in the upper 0.2 m as the SST (supporting information A). The field array was initially deployed near 115.3 °E and 16.8 °S on 22 November 2018 (figure 1). Three weeks later, the deep convection of an MJO event arrived in the eastern basin of the Indian Ocean, which was identified using the satellite-measured precipitation and outgoing longwave radiation anomalies (Feng *et al* 2020). Though this MJO was not weak based on the MJO index (www.bom.gov.au/climate/mjo/; Wheeler and Hendon 2004), the associated deep convection did not propagate across the Maritime Continent. According to the buoy measurements at 16.8 °S, the westerly wind increased after 10 December, but the precipitation remained zero. The deep convection of this MJO might propagate only along the equator instead of detouring to 15 °S.

Two ALAMO floats failed before 24 November. The remaining ALAMO (9205, 9207, 9209, and 9210) and EM-APEX (em8487 and em8488) floats initially drifted northwestward due to the geostrophic currents (black arrows in figure 1(a)). A strong cold-core cyclonic eddy was located just east of the float array. Four floats closer to the center of the eddy (9207, 9209, 9210 and em8488) then drifted around it to the northeast. All floats continuously profiled the upper 500 m ocean after 28 November except em8488. Float em8488 which profiled in the upper 250 m before 2 December, had a faster drifting speed than the other floats due to the effect of geostrophic current. The trajectories of 9207 and 9210 from 2 December to 6 December were similar to the trajectory of em8488 from 29 November to 30 November. The float array delivered a detailed evolution of the upper ocean stratification, which was useful for understanding how surface fluxes, ocean currents, and turbulent mixing might impact SST.

The peak of downward shortwave radiation at the buoy was >900 W m^{-2} (positive for downward heat fluxes) from 30 November to 6 December

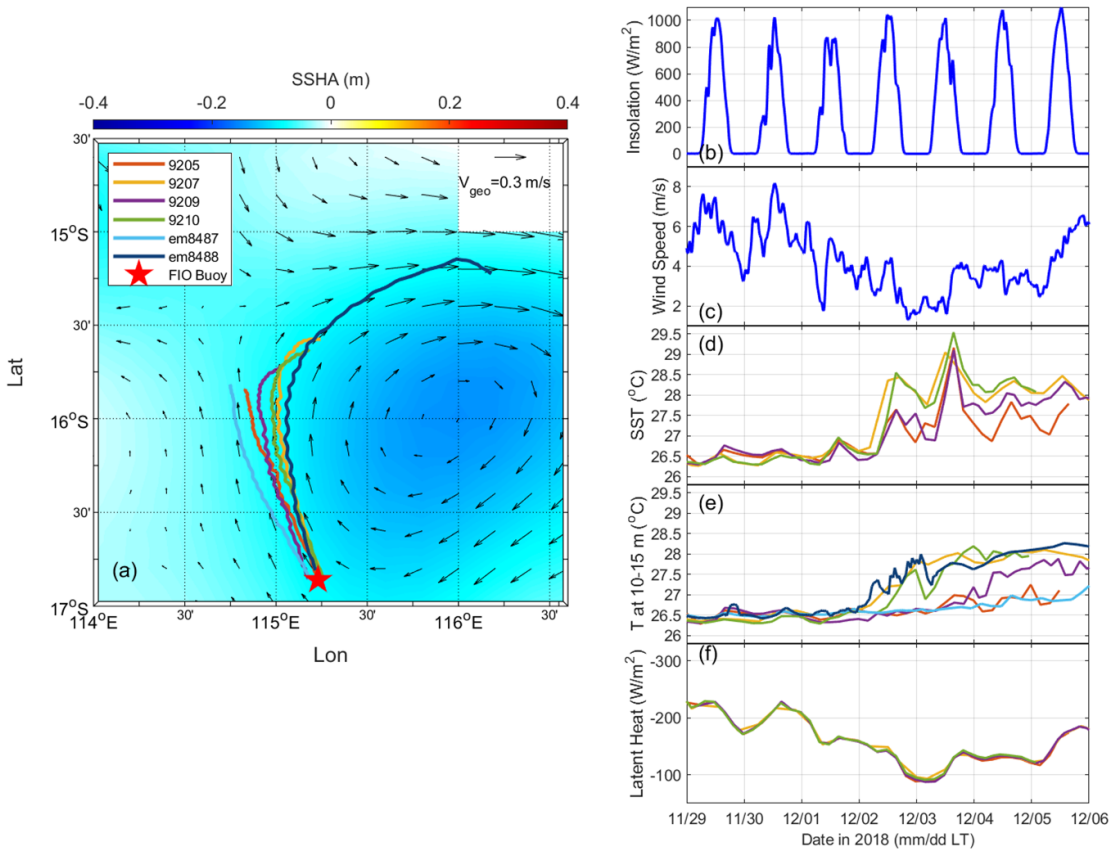

Figure 1. (a) Trajectories of four ALAMO floats (9205, 9207, 9209 and 9210; color lines) and two EM-APEX floats (em8487 and em8488; color lines) from deployment in 22 November to 6 December 2018. The position of the FIO buoy is shown as a red star; (b) downward solar radiation measured by the buoy; (c) wind speed at 4 m height above the sea surface; (d) measured SST by ALAMO floats; (e) the float-measured mean subsurface temperature from 10 to 15 m depth; and (f) the estimated latent heat flux using the COARE algorithm 3.0 (Fairall *et al* 1996, 2003). The color shading and black arrows in (a) are the sea surface height anomalies SSHA and geostrophic current V_{geo} from satellite measurements. The heat flux is positive downward.

(figure 1(b)). The wind speed at 4 m height above the sea surface was mostly >4 m s^{-1} before 2 December (figure 1(c)). The magnitude of **the diurnal variations of SST (DV SST,** defined as daytime peak minus nighttime minimum; figure 1(d)) was generally less than 0.5 °C before 2 December, because the strong wind could induce turbulent mixing for cooling SST (Thompson *et al* 2019). The wind speed decreased to a minimum of 2 m s^{-1} at midnight of 3 December. The extremely low wind speed and sunny days might explain why the DV SST could be >2 °C afterward. Interestingly, the nighttime minimum SST increased rapidly from 26.5 to 27.7 °C between 2 December and 4 December at all floats except 9205, within the same period when the strong DV SST occurred. For the EM APEX floats, the measured subsurface temperature variability in the range of 10–15 m depth (figure 1(e)) was similar to that captured by the nearby ALAMO floats.

We use the COARE 3.0 algorithm for computing the latent and sensible heat fluxes (Fairall *et al* 1996, 2003). The latent heat flux dropped from −220 to −100 W m^{-2} between 1 December and 3 December (figure 1(f)), because the wind speed decreased down to 2 m s^{-1}. Though the low wind speed suppressed the latent heat flux from 2 December to 4 December, the warming of daily-mean SST would eventually enhance the latent heat flux once the wind speed increases (Hsu *et al* 2019), e.g. the latent heat flux was up to −180 W m^{-2} at wind speed >6 m s^{-1} on 5 December. The relative humidity rose to more than 80% after 7 December (supporting information A). The rapid SST warming might enhance the 'efficiency' for accumulating air-sea heat fluxes and moisture during the suppressed phase of MJOs (Maloney 2009). The key question is, why did the rapid warming of daily-mean SST not occur until 3 December? This will be explored in the following analysis.

3. Restratification of the ocean surface boundary layer during the suppressed phase of MJOs

3.1. Definition of surface ML depth

Various criteria for estimating the depth of the ML (MLD) have been proposed (Sprintall and Roemmich 1999, de Boyer Montégut *et al* 2004, Suga *et al* 2004), such as finding the difference of potential density $\Delta\rho$ between ρ(MLD) and $\rho(z_0)$ exceeding some arbitrary constant (Chi *et al* 2014), where z_0

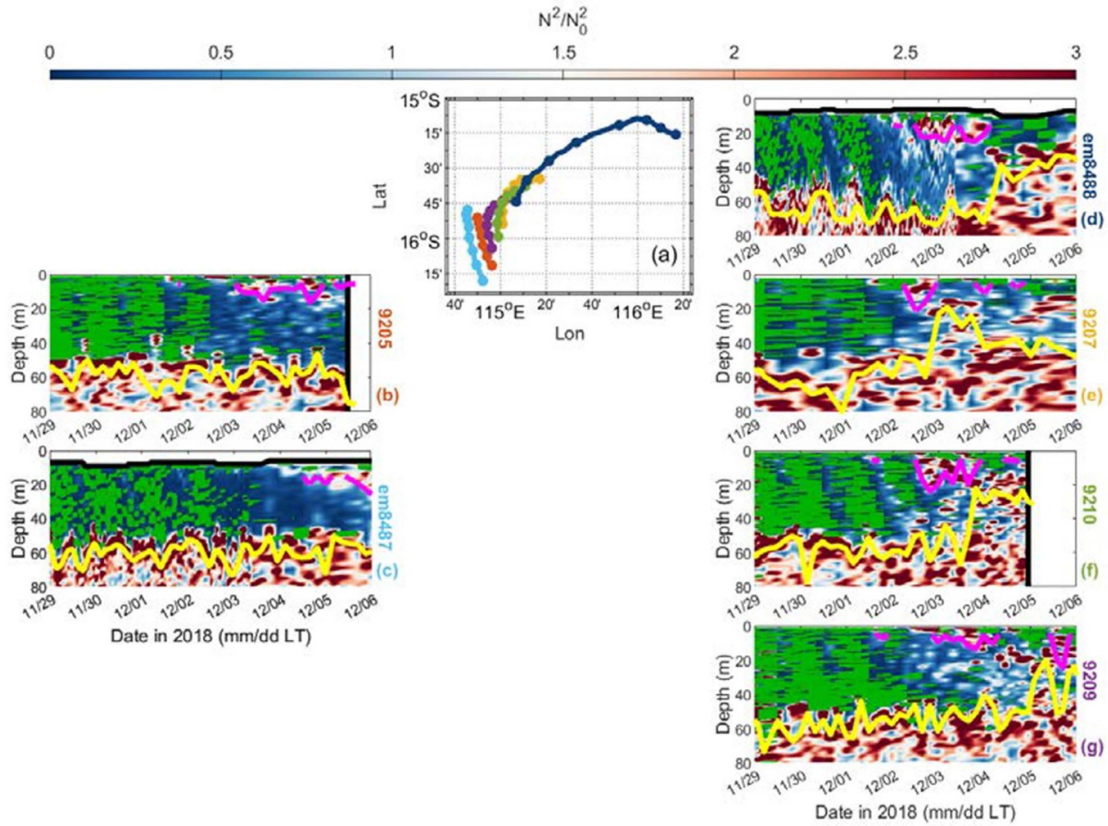

Figure 2. Float trajectories from 29 November to 5 December 2018 (color lines with dots in (a); labeled on the right of (b)–(g)), the measured buoyance frequency N^2 normalized by a constant N_0^2 of 1.0×10^{-4} s^{-2} at six floats (b)–(g). The interval between each color dot (the position of floats at 12 am each day) in (a) is one day. In (b)–(g), the green color marks the near zero or negative N^2 due to density inversions, and the magenta lines are the reference depth z_0 for estimating the surface mixed layer depth (MLD; yellow lines), which is computed as the bottom of the diurnal thermocline during diurnal warming. Only $z_0 > 5$ m at the ALAMO floats and $z_0 > 15$ m at the EM-APEX floats are shown. Missing measurements are indicated by white areas bounded by black lines in (c), (d), and at the right of the black line in (b), (f).

is the reference depth close to the ocean surface. The results of MLD (yellow lines in figure 2) in this study are thus estimated by fulfilling two criteria at the same time: potential density difference $\Delta\rho = \rho(\text{MLD}) - \rho(z_0) > 0.3$ kg m^{-3} and potential density gradient $\partial\rho/\partial z < -0.03$ kg m^{-4} (Hsu *et al* 2017), where the axis z is positive upward. Because of the sharp temperature gradient in the diurnal thermocline, the z_0 (magenta lines in figure 2) at the ALAMO floats is computed by finding the bottom of the diurnal thermocline, i.e. where vertical temperature gradients weaken to less than 0.02 °C m^{-1} over a 5 m span below 3 m depth. That is, the z_0 can also be used for identifying the thickness of the diurnal warm layer. The z_0 at the EM-APEX floats is estimated in the same way but starting from the 13 m depth (due to the missing upper 10 m measurements).

3.2. Observed evolution of stratification in the upper ocean

The strength of the ocean stratification was tracked by computing the buoyancy frequency N^2 ($=-(g/\rho)(\partial\rho/\partial z)$, where g is the gravity constant), normalized by a constant $N_0^2 = 1.0 \times 10^{-4}$ s^{-2}. Before 2 December, the MLD at all floats was about 60 m depth (yellow line figure 2), because the nighttime convective mixing eroded stratification above the MLD regularly (inversion of density $N^2 < 0$ shaded by the green dots in figure 2). Though the peak of downward solar radiation was mostly more than 900 W m^{-2} after 29 November (figure 1), a thick diurnal warm layer ($N^2/N_0^2 > 2$ in the upper 10 m) was not formed until 2 December, which was driven by the decreasing wind speed. The presence of the diurnal warm layer could inhibit turbulent mixing efficiently (Matthews *et al* 2014).

The RL, spanning from the bottom of the diurnal thermocline (magenta lines in figure 2) to the MLD (yellow lines), appeared during the period with strong diurnal SST warming. The N^2/N_0^2 within the RL varied significantly at different floats after 2 December. For the floats (9207, 9209, 9210, and em8488) drifting northeastward, the N^2/N_0^2 in the RL increased from 0.5 to more than 2.5. The shoaling of MLD was up to 40 m in two days, i.e. a rapid restratification of the ocean surface boundary layer. In contrast, the N^2/N_0^2 remained nearly constant at 0.5 at 9205 and em8487, which continuously drifted northward before 6 December. The warming of daily-mean SST at the ALAMO floats was in good agreement

with the shoaling of MLD. While that em8488 drifted faster and farther than the other three nearby ALAMO floats, the timing of the rapid shoaling of MLD was similar. The observed increase of SST and shoaling of MLD were unlikely due to the lateral heterogeneity in the ocean structure.

4. Regional oceanic modeling system (ROMS) simulations using the K-profile parameterization (KPP) mixing scheme

The rapid daily-mean SST warming within two days (>1 °C) might be associated with the restratification of the ocean surface boundary layer. Because the changes of MLD can affect the estimation of the upper ocean heat budget, it is unlikely to use *in-situ* oceanic measurements for identifying dominant factors in the change of near-surface temperature (Kunze *et al* 2021). To properly separate the effects of downward heat flux and horizontal advection, we use an ocean model for simulating the response of the upper ocean structure to the prescribed atmospheric forcing in the following.

4.1. Model setting

We use the KPP scheme (Shinoda and Hendon 1998, Bernie *et al* 2005, Kawai and Wada 2007) in the 3D (ROMS; Shchepetkin and McWilliams 2005) to simulate the evolution of upper ocean in the float array region. The temporal resolution is 10 min, and the horizontal resolution is 5 km. The vertical resolution is less than 1 m in the upper 20 m, in order to simulate the diurnal warming of SST reliably (Bernie *et al* 2005). The atmospheric measurements at the buoy, which are in good agreement with the reanalysis products (Dee *et al* 2011), are used for computing air-sea fluxes in the model via the COARE 3.0 algorithm (Fairall *et al* 1996, 2003), assuming spatially-homogeneous fluxes.

The GOFS 3.1 3dVar ocean state product (Cummings and Smedstad 2013), which assimilates available satellite and *in-situ* measurements (excluding our float data), is used as the initial conditions at midnight of 30 November. Because the float-measured temperature during the nighttime convective mixing is nearly homogeneous within the ML before 2 December, we use the float profiles during the nighttime from 28 November to 2 December (from 11 pm in the previous night to 5 am; Karagali and Høyer 2014) for implementing the initial conditions. Compared to the float observations (supporting information B), the GOFS product overestimates the salinity at all floats (>0.6 psu), and the mean subsurface temperature from 10 to 25 m depth at the north of 15.5 °S (>0.7 °C). The initial conditions are thus constructed by adjusting the difference to the GOFS product (supporting information C). The main purpose is to bring the initial conditions close to the float observations before strong diurnal variations of SST occur. The water mass structure around the float array then evolves based on the lateral advection and shear of ocean current (from GOFS), and the full observed air-sea fluxes.

4.2. Simulated SST and density stratification N^2 at the floats

We extract the simulated SST at the positions of the ALAMO floats (figure 3). The model results of SST warming are similar to the observations. However, the model slightly underestimates the DV SST captured by 9207 and 9210 on 2 December and 3 December, ∼0.6 °C. The choice of vertical mixing scheme and vertical resolution of the ocean model may affect the simulation of DV SST (Kawai and Wada 2007). We then compare the mean subsurface temperature from 10 to 15 m depth between the model results and observations. The difference is negligible at two EM-APEX floats. In other words, the model may have qualitatively reproduced the dynamics for increasing the temperature near the sea surface.

According to the simulated N^2/N_0^2 (figure 3), where ${N_0}^2$ is a constant of 1.0×10^{-4} s^{-2}, the model simulates a diurnal warm layer in the upper 5 m, but it is much thinner than that in the observations. Since 2 December, the model results of N^2/N_0^2 from 40 to 60 m depth can change by more than 1.5 at three ALAMO floats except 9205. The trend of the simulated density stratification in the upper ocean is similar to the observations, consistent with the model performance in simulating the SST warming. Before 2 December, the nighttime convective mixing can cause the density inversion ($N^2 < 0$) from the sea surface to more than 20 m depth. After 3 December, the simulated $N^2 < 0$ due to the nighttime convective mixing is mostly in the upper 10 m. The decrease of latent heat flux (figure 1) may weaken the simulated radiative cooling and nighttime convective mixing, as that found in the observations. The increase of N^2 in the upper ocean may also inhibit the turbulent mixing. On the other hand, the model fails to simulate the increase of N^2/N_0^2 from 20 to 60 m depth at em8488 after 5 December. The insufficient measurements at the north of 15.5 °S (figure 1) may affect the background ocean conditions of the model runs.

4.3. Factors to the simulated restratification in the upper ocean

Because of the qualitative agreement between the simulations and observations before 4 December, we will explore the dominant factors driving the simulated restratification of the ocean surface boundary layer at float 9209 first (figure 4). Based on the linear seawater density equation $\rho = \rho_0 + \rho_0(-\alpha(T - T_0) + \beta(S - S_0))$ (where the α and β are the expansion coefficients of heat and saline, respectively), we can explore the temporal change of density stratification $\partial N^2/\partial t$ (Johnson *et al* 2020), by using the temperature change rate due to

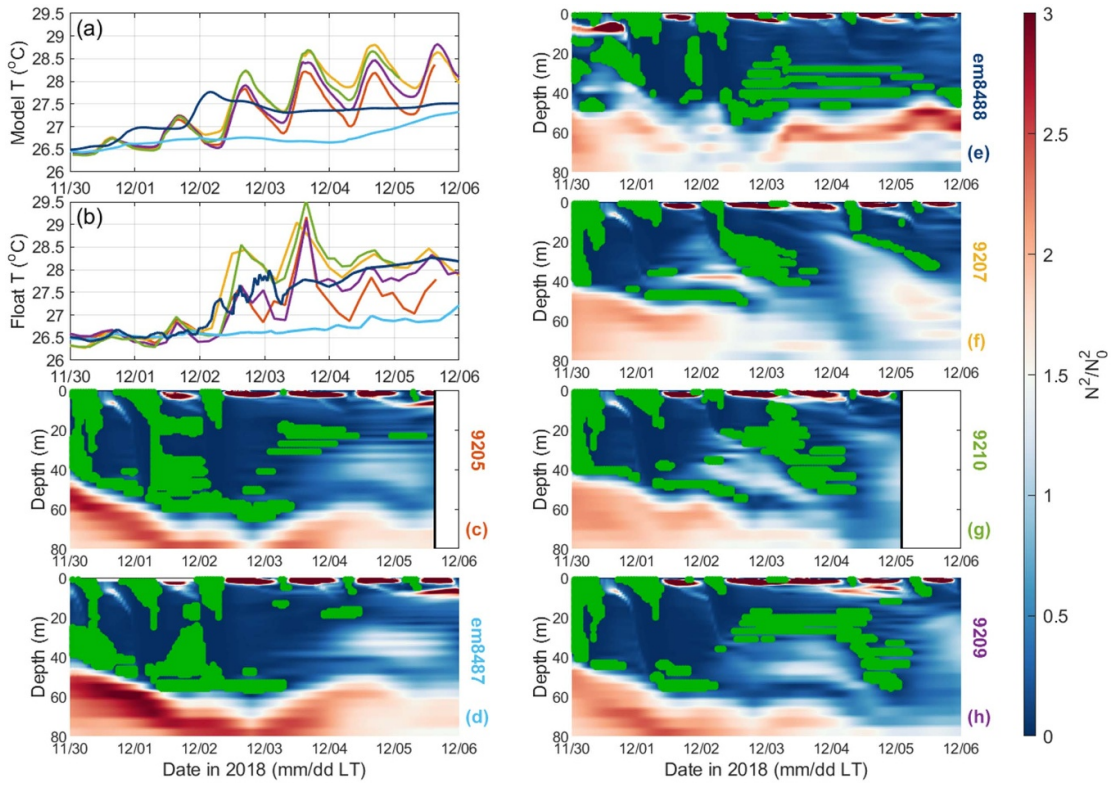

Figure 3. Model results (a) and observations (b) of SST at the ALAMO floats and mean subsurface temperature from 10 to 15 m depth at the EM-APEX floats (color lines, labeled at the right of (c)–(h)), respectively; (c)–(h) the simulated buoyance frequency N^2 normalized by a constant N_0^2 of 1.0×10^{-4} s^{-2}. The green color marks the negative N^2 due to the density inversion.

the horizontal advection ($\partial T_a/\partial t$) and vertical diffusion ($\partial T_d/\partial t$, which includes penetrative solar radiation), and salinity change rate due to the horizontal advection ($\partial S_a/\partial t$) and vertical diffusion ($\partial S_d/\partial t$), respectively. The contribution of temperature and salinity to the change of N^2 will be studied, assuming $\frac{\partial N^2}{\partial t} \approx g\frac{\partial}{\partial z}\left(\alpha\left(\frac{\partial T_a}{\partial t}+\frac{\partial T_d}{\partial t}\right)-\beta\left(\frac{\partial S_a}{\partial t}+\frac{\partial S_d}{\partial t}\right)\right)$.

Before midnight of 2 December, the nighttime convective mixing initialized by the heat loss destratifies the density stratification in the upper 40 m, though the temperature and salinity advection may have slightly restratified the RL in the upper 50 m during the daytime (figure 4). The T_d due to the nighttime convective mixing is much larger than the contribution from the other terms. After 2 December, the T_d favored by the strong insolation and low wind speed forms strong N^2 near the sea surface as a diurnal warm layer. Because the decreasing wind speed weakens the latent heat flux, the upward net heat flux decreases, so the radiative cooling is reduced. The weaker nighttime convective mixing is unable to erode the diurnal warm layer and RL formed during the daytime, in good agreement with Kunze *et al* (2021).

According to the cumulative change of N^2/N_0^2 since midnight of 30 November, i.e. $\Delta N^2/N_0^2$, the nighttime convective mixing does not destratify the N^2/N_0^2 after 2 December, consistent with the timing of decreasing wind speed. The simulated horizontal advection increases the N^2 of RL from 20 to 40 m depth, presumably due to the northeastward current at the northwest edge of the cold eddy (figure 1). The role of horizontal advection in restratifying the RL is consistent with that reported by Brainerd and Gregg (1993). We then explore the $\Delta N^2/{N_0}^2$ at float 9205 (supporting information D), which is farther away from the center of the cold eddy than 9209. Because the horizontal advection does not increase $\Delta N^2/N_0^2$ in the upper 50 m significantly before 3 December, the diffusion due to the nighttime convective mixing can still destratify the simulated N^2 of RL at 9205, even the atmosphere conditions between 9205 and 9209 should be similar. In other words, the formation of the diurnal warm layer and restratified RL may both affect the strength of nighttime convective mixing.

Based on the float observations and model results, we may conclude that a thick diurnal warm layer was formed near the sea surface, because the decreasing wind speed reduced the upward latent heat flux and shear instability mixing since 2 December. After the sunset, the net air-sea heat loss might cause less SST cooling and suppress the strength of nighttime convective mixing. Besides, the diurnal warm layer near the sea surface (e.g. Huang and Feng 2021) contribution of temperature might prevent the nighttime convective mixing from eroding the RL in the subsurface ocean. The subsurface RL could then be continuously restratified by the horizontal advection.

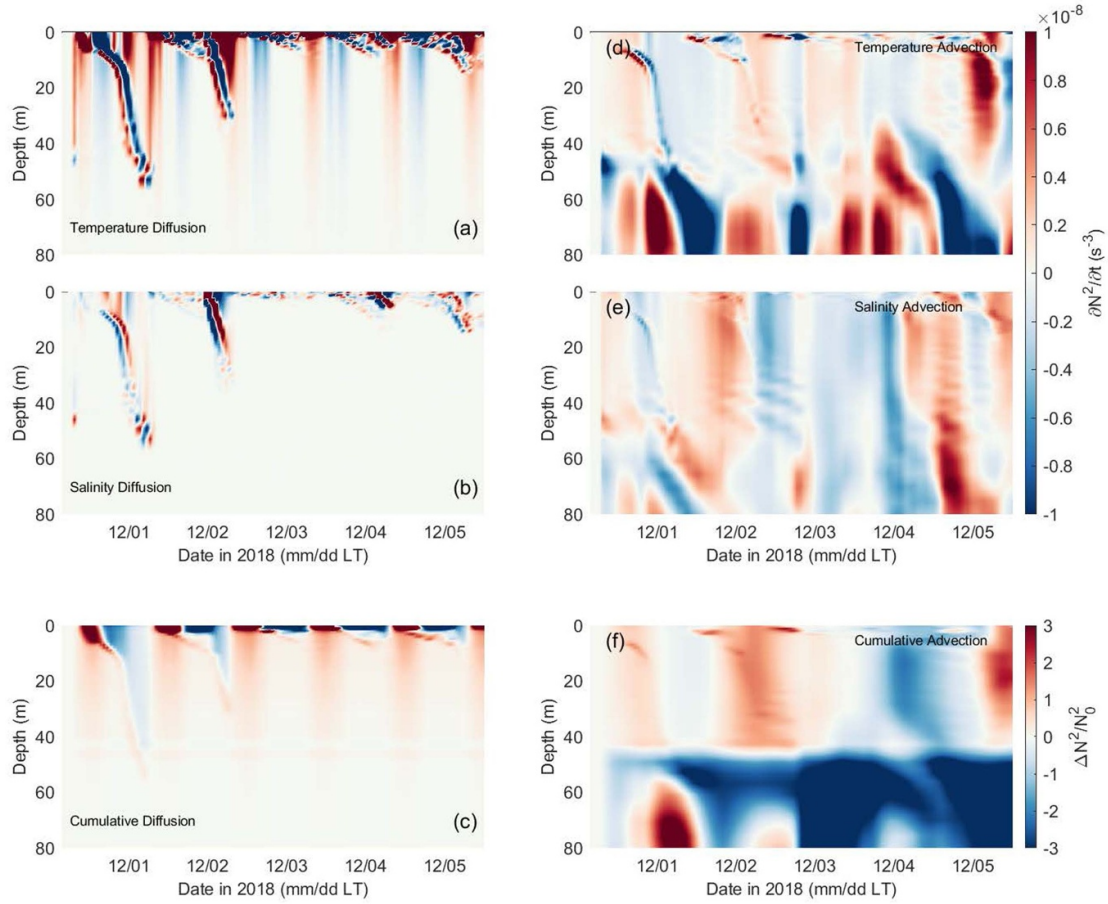

Figure 4. Contribution to the temporal change of density stratification $\partial N^2/\partial t$ from the temperature diffusion term: $g\alpha\partial(\partial T_d/\partial t)/\partial z$ (a), salinity diffusion term: $-g\beta\partial(\partial S_d/\partial t)/\partial z$ (b), temperature advection: $g\alpha\partial(\partial T_a/\partial t)/\partial z$ (d) and salinity advection: $-g\beta\partial(\partial S_a/\partial t)/\partial z$ (e) at float 9209 by using the model output from ROMS. The cumulative change of $\Delta N^2/N_0^2$ since midnight of 30 November due to the vertical diffusion and horizontal advection is presented in (c) and (f), respectively.

Once the upper ocean was restratified, the verical mixing might not entrain the cold water from the subsurface ocean efficiently, even when the wind speed was restrengthened to more than 4 m s^{-1}. The heat trapped in a shallow layer near the sea surface increased the daily-mean SST. Therefore, the decreasing wind speed and restratified upper ocean since 2 December could explain the rapid warming of daily-mean SST since 3 December (section 2).

5. Discussion on the roles of upper ocean restratification in MJO-ocean interaction

Though the dynamics initialized by the low wind speed and clear sky during the seasonal transition of ML may be found in other regions (Kunze *et al* 2021), these two conditions are the key features driven by the atmospheric general circulation of MJOs across the Indian Ocean. MJOs as intraseasonal weather systems propagating eastward along the equator may facilitate the seasonal transition of the ocean surface boundary layer around the Maritime Continent. The restratified upper ocean can inhibit turbulent mixing for entraining cold water from subsurface layers, so the SST warms rapidly. On the other hand, though the importance of horizontal advection in the large-scale MJO-ocean interaction has been demonstrated previously (e.g. Marshall and Hendon 2014), the effect of horizontal advection on the restratification of upper ocean under a stable atmosphere condition may also be crucial. Because MJOs are multi-scale weather systems, understanding the complicated interaction between the upper ocean and atmospheric conditions during different phases of MJOs may benefit the prediction of the lifetime of these intraseasonal weather systems.

Except for the strength of MJOs' deep convections, factors influencing the propagation trajectories of MJOs near the Maritime Continent (MC) are extensively explored by several recent studies (e.g. Zhang and Ling 2017), because not all MJOs can propagate across the MC. The MJOs sometimes detour southward before passing the MC (Zhou and Murtugudde 2020). Though the dynamics have not been fully understood, some studies hypothesize that the SST at the eastern basin of the Indian Ocean may affect the accumulation of heat and moisture in the lower troposphere (e.g. Zhang and

Ling 2017). According to the buoy measurements in this experiment, the downwelling due to the suppressed phase of MJOs may affect the weather conditions far away from the equator. In other words, exploring the spatial variation of horizontal advection of ocean current around the northwest shelf of Australia may also affect model forecasts on the trajectories of MJOs.

6. Summary and conclusions

During the suppressed phase of one MJO event in the middle of December 2018 (Feng *et al* 2020), four ALAMO floats and two EM-APEX floats were deployed off northwest Australia. The observed diurnal variation of SST was up to 2 °C under low wind speed (∼2 m s^{-1}) and sunny conditions since 2 December. A thick diurnal warm layer was formed near the sea surface. After the occurrence of strong diurnal variation of SST, the N^2/N_0^2 at three ALAMO floats and one EM-APEX float increased from less than 0.5 to more than 2.5 in the upper 50 m, and shoaled MLD by at least 20 m in two days. We observed a rapid restratification of the ocean surface boundary layer during the suppressed phase of an MJO. The restratified layers then sustained a high SST > 27.5 °C until the onset of MJO convections (Feng *et al* 2020). On the other hand, the daily-mean SST and upper ocean stratification at the other two floats did not change significantly during this period, presumably due to the spatial variation of horizontal advection.

We used the KPP mixing scheme in the 3D ROMS model for simulating the dynamics in this restratification process. The model results of SST and N^2/N_0^2 in the upper ocean were consistent with our observations. Though the simulated horizontal advection of temperature and salinity could slightly restratify the subsurface ocean before 1 December, strong nighttime mixing still eroded all density stratification above the MLD. Since 2 December, the extremely low wind speed favored the formation of a thick diurnal warm layer by decreasing the latent heat flux, which could stabilize the upper ocean. The simulated nighttime convective mixing weakened by the reduced upward heat loss was therefore unable to destratify the layers formed during daytime. It prolonged the period for the upper ocean restratified by the horizontal advection and penetrative solar radiation, consistent with that reported by Kunze *et al* (2021). In other words, this rapid restratification process was initialized by the atmospheric conditions of low wind speed and sunny days. The increased near-surface stratification would reduce the turbulent mixing due to the downward turbulent flux so that the subsurface layers could be continuously restratified by the horizontal advection. Because more heat was trapped within a shallower near-surface layer, the observed daily-mean SST was warmed rapidly by more than 0.5 °C since 3 December. The accumulation of heat and moisture in the atmospheric boundary layer, modulated by the SST variations, could affect the onset and development of MJOs' deep convection (e.g. Maloney 2009, Seo *et al* 2014).

In summary, a stable sunny atmosphere with low wind speeds during the suppressed phase of MJOs may be favorable to the restratification of the ocean surface boundary layer near the MC around the austral spring. Low latent heat flux due to the extremely low wind speed may result in strong diurnal variations of SST and formation of the diurnal warm layer, and then reduce the strength of nighttime convective mixing. Because the nighttime convective mixing is suppressed, the near-surface layers can be continuously restratified by the horizontal advection and penetrative solar radiation. The increase of density stratification in the upper ocean may sustain high SST, air-sea heat and moisture fluxes until the onset of the MJOs convective phase (Maloney 2009). Field measurements on turbulent diffusivity within the stratified layers in TWPs are essential for improving the ocean mixing approaches, even future used in the global coupled models for the MJO forecast.

Data availability statement

The data that support the findings of this study are openly available at the following URL/DOI: https://doi.org/10.25919/5da51c424add0. Data will be available from 15 October 2022.

Acknowledgments

This work is funded by the project of 'Coupled warm pool dynamics in the Indo-Pacific' under the CSHOR. CSHOR is a joint initiative between the Qingdao National Laboratory for Marine Science and Technology (QNLM), CSIRO, University of New South Wales and University of Tasmania. The authors thank the GOFS 3.1 product (https://tds.hycom.org/thredds/catalogs/GLBv0.08/expt_93.0.html), IMOS portal for processing the dataset of sea surface height anomalies in the dataset 'IMOS—OceanCurrent—Gridded sea level anomaly—Delayed mode' (https://portal.aodn.org.au/), N Bogue and R Nigash at MRV for helping configure and pilot the floats, D Slawinski (CSIRO) and P Robbins (WHOI) for post-processing the float measurements. Float data is stored at 10.25919/5da51c424add0.

ORCID iD

Je-Yuan Hsu https://orcid.org/0000-0002-4229-2633

References

Bernie D J, Guilyardi E, Madec G, Slingo J M, Woolnough S J and Cole J 2008 Impact of resolving the diurnal cycle in an ocean–atmosphere GCM. Part 2: a diurnally coupled CGCM *Clim. Dyn.* **31** 909–25

Bernie D J, Woolnough S J, Slingo J M and Guilyardi E 2005 Modeling diurnal and intraseasonal variability of the Ocean mixed layer *J. Clim.* **18** 1190–202

Boccaletti G, Ferrari R and Fox-Kemper B 2007 Mixed-layer instabilities and restratification *J. Phys. Oceanogr.* **37** 2228–50

Brainerd K E and Gregg M C 1993 Diurnal restratification and turbulence in the oceanic surface mixed layer: 1. Observations *J. Geophys. Res. Oceans* **98** 22645–56

Brainerd K E and Gregg M C 1995 Surface mixed and mixing layer depths *Deep-Sea Res.* I **42** 1521–43

Chi N-H, Lien R-C, D'Asaro E A and Ma B B 2014 The surface mixed layer heat budget from mooring observations in the central Indian Ocean during Madden–Julian oscillation events *J. Geophys. Res. Oceans* **119** 4638–52

Cole R, Kinder J, Chun Lin N, Yu W and Chao Y 2011 'Bai-Long': a TAO-hybrid on RAMA *Oceans'11 MTS/IEEE KONA* (*Waikoloa, HI*) pp 1–10

Cummings J A and Smedstad O M 2013 Variational data assimilation for the global Ocean *Data Assimilation for Atmospheric, Oceanic and Hydrologic Applications* vol II ch 13, pp 303–43 (https://ieeexplore.ieee.org/document/6106952)

de Boyer Montégut C, Madec G, Fischer A S, Lazar A and Iudicone D 2004 Mixed layer depth over the global ocean: an examination of profile data and a profile-based climatology *J. Geophys. Res.* **109** C12003

Dee D P *et al* 2011 The ERA-Interim reanalysis: configuration and performance of the data assimilation system *Q. J. R. Meteorol. Soc.* **137** 553–97

DeMott C A, Klingaman N P and Woolnough S J 2015 Atmosphere-ocean coupled processes in the Madden–Julian oscillation *Rev. Geophys.* **53** 1099–154

Fairall C W, Bradley E F, Hare J E, Grachev A A and Edson J B 2003 Bulk parameterization of air-Sea fluxes: updates and verification for the COARE algorithm *J. Clim.* **16** 571–91

Fairall C W, Bradley E F, Rogers D P, Edson J B and Young G S 1996 Bulk parameterization of air-sea fluxes for tropical ocean-global atmosphere coupled-ocean atmosphere response experiment *J. Geophys. Res.* **101** 3747–64

Feng M *et al* 2020 Tracking air-sea exchange and upper ocean variability in the Southeast Indian Ocean during the onset of the 2018-19 Australian summer monsoon *Bull. Am. Meteorol. Soc.* **10** E1397–412

Fox-Kemper B and Ferrari R 2008 Parameterization of mixed-layer eddies 2: prognosis andimpact *J. Phys. Oceanogr.* **38** 1166–79

Hsu J Y, Hendon H, Feng M and Zhou X 2019 Magnitude and phase of diurnal SST variations in the ACCESS-S1 model during the suppressed phase of the MJOs *J. Geophys. Res. Oceans* **124** 9553–71

Hsu J-Y, Lien R-C, D'Asaro E A and Sanford T B 2017 Estimates of surface wind stress and drag coefficients in typhoon megi *J. Phys. Oceanogr.* **47** 545–65

Huang Z and Feng M 2021 MJO induced diurnal sea surface temperature variations off the northwest shelf of Australia observed from Himawari geostationary satellite *Deep-Sea Res.* II **183** 104925

Hughes K G, Moum J N and Shroyer E L 2020 Evolution of the velocity structure in the diurnal warm layer *J. Phys. Oceanogr.* **50** 615–31

Jerlov N G 1976 *Marine Optics* (*Elsevier Oceanography Series* vol 14)

Johnson L, Lee C M and D'Asaro E A 2016 Global estimates of lateral springtimerestratification *J. Phys. Oceanogr.* **46** 1555–73

Johnson L, Lee C M, D'Asaro E A, Thomas L and Shcherbina A 2020 Restratification at aCalifornia Current upwelling front 1: observations *J. Phys. Oceanogr.* **50** 1455–72

Karagali I and Høyer J L 2014 Characterisation and quantification of regional diurnal SST cycles from SEVIRI *Ocean Sci.* **10** 745–58

Kawai Y and Wada A 2007 Diurnal sea surface temperature variation and its impact on the atmosphere and ocean: a review *J. Oceanogr.* **63** 721–44

Kudryavtsev V N and Soloviev A V 1990 Slippery near-surface layer of the Ocean arising due to daytime solar heating *J. Phys. Oceanogr.* **20** 617–28

Kunze E, Mickett J B and Girton J B 2021 Destratification and restratification of the spring surface boundary layer in a subtropical front *J. Phys. Oceanogr.* **51** 2861–82

Large W G, McWilliams J C and Doney S C 1994 Oceanic vertical mixing: a review and a model with a nonlocal boundary layer parameterization *Rev. Geophys.* **32** 363–403

Mahadevan A, D'Asaro E A, Lee C M and Perry M J 2012 Eddy-driven stratificationinitiates North Atlantic spring phytoplankton blooms *Science* **337** 54–58

Mahadevan A, Tandon A and Ferrari R 2010 Rapid changes in mixed layer stratification driven by submesoscale instabilities and winds *J. Geophys. Res. Oceans* **115** C03017

Maloney E D 2009 The moist static energy budget of a composite tropical intraseasonal oscillation in a climate model *J. Clim.* **22** 711–29

Marshall A G and Hendon H H 2014 Impacts of the MJO in the Indian Ocean and on the Western Australian coast *Clim. Dyn.* **42** 579–95

Matthews A J, Baranowski D B, Heywood K J, Flatau P J and Schmidtko S 2014 The surface diurnal warm layer in the Indian Ocean during CINDY/DYNAMO *J. Clim.* **27** 9101–22

Moulin A J, Moum J N and Shroyer E L 2018 Evolution of turbulence in the diurnal warm layer *J. Phys. Oceanogr.* **48** 383–96

Moum J N *et al* 2014 Air–Sea interactions from westerly wind bursts during the November 2011 MJO in the Indian Ocean *Bull. Am. Meteorol. Soc.* **95** 1185–99

Paulson C A and Simpson J J 1977 Irradiance measurements in the upper ocean *J. Phys. Oceanogr.* **7** 952–6

Ruppert J H and Johnson R H 2015 Diurnally modulated cumulus moistening in the preonset stage of the Madden–Julian oscillation during DYNAMO *J. Atmos. Sci.* **72** 1622–47

Seo H, Subramanian A C, Miller A J and Cavanaugh N R 2014 Coupled impacts of the diurnal cycle of Sea surface temperature on the Madden–Julian oscillation *J. Clim.* **27** 8422–43

Shchepetkin A F and McWilliams J C 2005 The regional oceanic modeling system (ROMS) a split-explicit, free-surface, topography-following-coordinate oceanic model *Ocean Model.* **9** 347–404

Shinoda T and Hendon H H 1998 Mixed layer modeling of intraseasonal variability in the tropical Western Pacific and Indian Oceans *J. Clim.* **11** 2668–85

Sprintall J and Roemmich D 1999 Characterizing the structure of the surface layer in the Pacific Ocean *J. Geophys. Res.* **104** 23297–311

Suga T, Motoki K, Aoki Y and Macdonald A M 2004 The North Pacific climatology of winter mixed layer and mode waters *J. Phys. Oceanogr.* **34** 3–22

Sui C, Li X, Lau K and Adamec D 1997 Multiscale Air–Sea Interactions during TOGA COARE *Mon. Wea. Rev.* **125** 448–62

Sutherland G, Marié L, Reverdin G, Christensen K H, Broström G and Ward B 2016 Enhanced turbulence associated with the diurnal jet in the Ocean surface boundary layer *J. Phys. Oceanogr.* **46** 3051–67

Thompson E J, Moum J N, Fairall C W and Rutledge S A 2019 Wind limits on rain layers and diurnal warm layers *J. Geophys. Res. Oceans* **124** 897–924

Wheeler M C and Hendon H H 2004 An all-season real-time multivariate MJO index: development of an index for monitoring and prediction *Mon. Wea. Rev.* **132** 1917–32
Zhang C 2005 Madden–Julian oscillation *Rev. Geophys.* **43** RG2003
Zhang C and Ling J 2017 Barrier effect of the Indo-Pacific maritime continent on the MJO: perspectives from tracking MJO precipitation *J. Clim.* **30** 3439–59
Zhou L and Murtugudde R 2020 Oceanic impacts on MJOs detouring near the maritime continent *J. Clim.* **33** 2371–88